Evolution of phonon-focusing caustics under linear spatial dispersion

2000 J. Phys. A: Math. Gen. 33 5105

(http://iopscience.iop.org/0305-4470/33/28/313)

J. Phys. A: Math. Gen. **33** (2000) 5105–5116. Printed in the UK PII: S0305-4470(00)12633-2

Evolution of phonon-focusing caustics under linear spatial dispersion

A L Shuvalov† and A G Every
Department of Physics, University of the Witwatersrand, Johannesburg 2001, South Africa

Received 14 March 2000

Abstract. Linear dispersion of elastic constants in non-centrosymmetric crystals has the effect of lifting phase-velocity degeneracy along those acoustic axes which do not lie in symmetry planes. The separating of the sheets of the isofrequency (or slowness) surface, even though slight at low frequencies, nevertheless has a striking effect on the phonon intensity pattern near to the removed degeneracy. Phonon focusing abides by the shape of the slowness surface, whose curvature is singular at the degeneracy point. Hence, a small perturbation breaking the degeneracy entails a large change of the curvature in a small region scaling in size with the magnitude of the perturbation. As a result, new phonon focusing caustics may arise, and existing caustics may undergo major changes near acoustic axes. Theoretical analysis reveals possible patterns of local transformation of the slowness surface leading to different types of critical behaviour of phonon focusing. Criteria, in terms of the elastic constants of a given crystal, are obtained for the emergence of focusing caustics.

1. Introduction

In non-centrosymmetric crystals lacking symmetry planes, the slight frequency dispersion of acoustic phonons at long wavelengths $\lambda \gg a$ (a is the lattice parameter) gives rise to striking features in ballistic phonon-focusing patterns. This is due to the fact that in such crystals dispersion has the effect of breaking the degeneracy between sheets of the constant frequency surface.

Phonon group-velocity vectors are orthogonal to their constant frequency surface and hence their distribution, which governs the phonon-intensity pattern, depends on this surface's curvature. From the theory of phonon imaging [1], it is known that the degree of phonon focusing is inversely proportional to the Gaussian curvature of the constant-frequency surface; in particular, lines of zero Gaussian curvature yield focusing caustics where the phonon energy flux diverges. Near degeneracy points the curvature is singular, and therefore a small perturbation-lifting degeneracy may have a dramatic impact on a focusing pattern. Some of the effects thereby arising have been discussed in [2]. It was demonstrated that lifting of a conical contact between isofrequency sheets in the direction of a 3-fold axis either brings about a new focusing caustic or extensively modifies the existing ones. It was also noted that lifting of a tangential degeneracy along a 4-fold axis may tear apart caustics intersecting at the degeneracy point. In the present paper we explore the theoretical basis of these and other effects of linear dispersion, such as dispersion-induced external conical refraction at a 6-fold axis and new focusing caustics around a 4-fold axis. The critical conditions for emergence of various phonon-focusing patterns are identified, and their evolution with frequency is described.

† Permanent address: Institute of Crystallography, Leninskii pr. 59, Moscow 117333, Russia.

0305-4470/00/285105+12$30.00

2. Background

Utilizing the framework of continuum elasticity for ballistic propagation of low-frequency acoustic phonons in non-dissipative anisotropic solids lacking a centre of inversion yields the dispersion equation in the form

$$\det\left[(c_{ijkl} + \mathrm{i}d_{ijklp}k_p)m_j m_l - \rho v^2 \delta_{ik}\right] = 0 \tag{1}$$

where ρ is the density, c_{ijkl} the elasticity coefficients, $\boldsymbol{k}$ the wavevector, v the phase velocity, $\boldsymbol{m}$ the unit wave normal, $d_{ijklp} = -d_{klijp}$ the coefficients of linear spatial dispersion, which are of relative magnitude $kd/\rho v^2 \sim ka \ll 1$ [3, 4]. The constant-frequency (isofrequency) surface $\omega =$ constant consists of three sheets Ω_α representing the two-parameter locus of wavevectors $\boldsymbol{k}_\alpha(\boldsymbol{m}) = \boldsymbol{m}\omega/v_\alpha$. Usually, the innermost sheet is associated with the quasilongitudinal wave branch ($\alpha = l$) and so the other two sheets correspond to quasitransverse branches (fast $\alpha =$ ft and slow $\alpha =$ st). The slowness surface is introduced as $S_\alpha = \omega^{-1}\Omega_\alpha : \boldsymbol{s}_\alpha(\boldsymbol{m}) = \boldsymbol{m}/v_\alpha$, whence its principal curvatures $K_1^{(\alpha)}$, $K_2^{(\alpha)}$ are ω^{-1} times those of the isofrequency surface. The lines separating regions with a different sign of the Gaussian curvature $K_G^{(\alpha)} = K_1^{(\alpha)}K_2^{(\alpha)}$ (parabolic lines where $K_G^{(\alpha)} = 0$) map onto phonon-focusing line caustics. In the absence of dispersion, the innermost slowness sheet S_l is always convex ($K_1^{(l)}$, $K_2^{(l)} > 0$), while any of the other two sheets S_α, $\alpha =$ st, ft, may include hyperbolic ($K_G^{(\alpha)} < 0$) and/or concave ($K_1^{(\alpha)}$, $K_2^{(\alpha)} < 0$) regions. There are directions, termed acoustic axes, for which the velocities of two waves (usually the quasitransverse ones) coincide and hence two slowness sheets S_{st}, S_{ft} meet. This meeting is of a conical type along 3-fold symmetry axes and in the case of a non-symmetrical orientation of acoustic axis, and it is of a smooth tangential type along 4-fold and 6-fold symmetry axes. Except for the case of 6-fold axes, the Gaussian curvature of the slowness surface is singular at a degeneracy point (it depends on the approaching path). As a result, parabolic lines may weave around and through a degeneracy point, thereby imposing intricate configurations of phonon-focusing caustics [5–7].

In the non-dispersive limit, the phase velocities $v_{0\alpha}$ in a given crystal depend solely on the wave normal orientation $\boldsymbol{m}$, and therefore the isofrequency surfaces for different frequencies are all identical in shape to the slowness surface, differing from it only by a scaling factor ω. Taking spatial dispersion into account implies that the phase velocity becomes frequency dependent, $v_\alpha = v_\alpha(\omega, \boldsymbol{m})$, the dependence following from (1) in which k may be approximated by $\omega/v_{0\alpha}$. The shape of the isofrequency surfaces now changes with varying ω, and hence so does the shape of the slowness surfaces referred to different constant frequencies. Note, in particular, that the innermost sheet S_l may, in principle, become locally hyperbolic or concave at some ω. However, dispersion-induced distortion of slowness surfaces in an arbitrary direction remote from degeneracy is relatively small (on the order of $(ka)^2 \ll 1$). The impact of linear dispersion becomes critical where it lifts the phase-velocity degeneracy. This happens if the degeneracy direction, referred to the non-dispersive limit, does not lie in a symmetry plane; in particular, if it occurs along a principal symmetry axis in any of the symmetry groups 3, 32, 4, 422, 6, 622, 23, 432 [3, 8]. Analysis of the ensuing critical features of the phonon-intensity patterns is the subject of the following discussion.

3. 3-fold axis

In the absence of dispersion, a 3-fold axis provides a conical degeneracy between the slowness sheets S_α ($\alpha =$ st, ft). At the conical point one of the principal curvatures for each of the

sheets diverges as

$$K_2^{(\mathrm{ft})} = -K_2^{(\mathrm{st})} \sim \theta^{-1} \tag{2}$$

where θ is the angle between the wave normal $\boldsymbol{m}$ and the symmetry axis. This brings about a phonon-intensity anticaustic (zero of intensity) at the circle of internal conical refraction [9]. The other principal curvature, $K_1^{(\alpha)}$, which is referred to the sections by family of planes through the 3-fold axis, is undefined at the conical point. Its limiting value as $\theta \to 0$ depends on the azimuth angle φ in accordance with† [7]

$$K_1^{(\alpha)}(\varphi) = \frac{1}{\sqrt{\rho c_{44}}\left[1 + (c_{14}/c_{44})^2\right]^{3/2}} C_\alpha(\varphi) \qquad \alpha = \mathrm{st}, \mathrm{ft} \tag{3}$$

where

$$C_\alpha(\varphi) = c_{66} - \frac{c_{14}^2}{c_{44}} + \frac{1}{2}\left(\Delta_{16} - \frac{d_{13}^2}{\Delta_{34}}\right)\left[1 \mp (\operatorname{sgn} c_{14}) \sin 3\varphi\right] \qquad \alpha = \mathrm{st}, \mathrm{ft} \tag{4}$$

upper and lower signs corresponding to $\alpha = \mathrm{st}$ and ft, respectively; the notation is

$$\Delta_{ab} = c_{aa} - c_{bb} \quad (a, b = 1, \ldots, 6) \qquad d_{ij} = c_{ijij} + c_{iijj} \quad (i, j = 1, 2, 3). \tag{5}$$

Associated with a sign of $K_1^{(\alpha)}(\varphi)$, there follow two possibilities for the local shape of the sheets S_α:

(a) if

$$c_{11} - \frac{c_{14}^2}{c_{44}} - \frac{d_{13}^2}{\Delta_{34}} > 0 \tag{6}$$

then $C_{\mathrm{st}}(\varphi)$, $C_{\mathrm{ft}}(\varphi)$ are positive for all φ, hence so are $K_1^{(\mathrm{st})}(\varphi)$, $K_1^{(\mathrm{ft})}(\varphi)$, whence the outer sheet S_{st} is hyperbolic and the inner sheet S_{ft} is convex around the conical point;

(b) alternatively, if

$$c_{11} - \frac{c_{14}^2}{c_{44}} - \frac{d_{13}^2}{\Delta_{34}} < 0 \tag{7}$$

then $C_\alpha(\varphi)$ and hence $K_1^{(\alpha)}(\varphi)$ ($\alpha = \mathrm{st}, \mathrm{ft}$) change signs with varying φ, so S_{st} has alternating hyperbolic/concave segments, S_{ft} has alternating convex/hyperbolic segments, and the parabolic lines separating those segments skip from one of the sheets to the other at the conical point. (Note that $C_\alpha(\varphi)$ cannot be negative for all φ because of the elastic-stability condition $c_{66}c_{44} > c_{14}^2$.)

Consider any one of the symmetry classes 3, 32, 23, 432, for which linear dispersion breaks the degeneracy along a 3-fold axis. On general grounds, it is evident that the resulting rounding of a conical point always renders the outer sheet S_{st} concave and the inner sheet S_{ft} convex within the close neighbourhood of the axis [2, 10]. Also clear is that outside a certain critical region near the axis, the curvature values may be approximated by the non-dispersive limit (2) and (3). Hence, in case (a) there is a new concave domain enclosing the 3-fold axis on the sheet S_{st} which is surrounded by a hyperbolic region, and separating these is a closed parabolic line that gives rise to an initially circular phonon-focusing caustic. In case (b) the parabolic lines, which were intersecting at the conical point in the non-dispersive limit, now

† It is referred to the case of a 3-fold axis in a trigonal crystal, in which $c_{25} = 0$ for symmetry reasons or due to the appropriate choice of the coordinate axis X_1. All the results of this section can be adapted for a cubic crystal by the standard replacement of elastic coefficients (e.g. [7]).

link up in pairs away from the 3-fold axis, and thereby the phonon-focusing pattern consisting of interchanging caustics of two quasitransverse branches disbands into a separate caustic for each of the branches, as demonstrated in [2]. Let us now provide the analytical framework describing the above-mentioned effects.

The perturbation-theory expansion for the phase velocities near the 3-fold axis may be written in the form

$$\rho v_\alpha^2 = c_{44} + \frac{1}{2}\left(\Delta_{14} - \Delta_{46} - \frac{d_{13}^2}{\Delta_{34}}\right)\theta^2 \mp \sqrt{4c_{14}^2\theta^2 + c_{44}^2\eta^2 + 2c_{14}\left(\Delta_{16} - \frac{d_{13}^2}{\Delta_{34}}\right)\theta^3 \sin 3\varphi} \qquad \alpha = \text{st, ft.} \tag{8}$$

Here η is the dimensionless parameter, which is proportional to the linear-dispersion coefficient $d_{13233} \equiv d_{543}$ and is equal to the relative difference between the squared phase velocities induced along the acoustic axis by the linear dispersion,

$$\eta = \frac{k_{0d}}{c_{44}}\,|d_{543}| = \frac{v_{\text{ft}}^2 - v_{\text{st}}^2}{v_{0d}^2} \qquad (0 < \eta \sim ka \ll 1) \tag{9}$$

where $k_{0d} = \omega/v_{0d}$ and $v_{0d} = \sqrt{c_{44}/\rho}$ is the degenerate phase velocity in the non-dispersive limit. For the wave normal directions so close to the 3-fold axis that $\theta \ll ka$, the principal curvatures for each of the sheets S_{st}, S_{ft} neglecting terms $\sim ka \ll 1$ are equal: $K_1^{(\alpha)} = K_2^{(\alpha)}$, $\alpha = \text{st, ft}$, and

$$K_{1,2}^{(\text{st})} = -K_{1,2}^{(\text{ft})} = -\frac{2v_{0d}}{\eta}\tan^2\Theta_0 \tag{10}$$

where $\Theta_0 = \arctan(c_{14}/c_{44})$ is the apex half-angle of the cone of internal refraction. On further deviation of the wave normal, yet remaining near the axis ($\theta \ll 1$), the curvature $K_2^{(\alpha)}$ steadily decreases its large absolute value given by (10) and then by (2); whereas $K_1^{(\alpha)}$ changes from (10) abruptly, tending to the value approximated by (3). The equation $K_1^{(\alpha)}(\theta, \varphi) = 0$ ($\alpha = \text{st, ft}$), in an approximation for small θ, has the following solution:

$$\theta_\alpha^3(\varphi) = \pm\frac{c_{44}^2}{4\,|c_{14}|\,C_\alpha(\varphi)}\eta^2 \qquad \alpha = \text{st, ft} \tag{11}$$

(upper and lower signs corresponding to $\alpha = \text{st, ft}$, respectively), where only positive values of θ_α make sense.

In case (a), which implies that $C_\alpha(\varphi) > 0$ at any φ (see (6)), equation (11) defines the closed parabolic line $\theta_{\text{st}}(\varphi) \sim \eta^{2/3}$ arising on the outer slowness sheet S_{st} due to linear dispersion. Mapping of this parabolic line onto the group-velocity manifold ($\theta_{\text{st}}(\varphi), \varphi \to \Theta, \Phi$) gives the folding line of the emerging phonon-focusing caustic. Its angular extent $\Theta_{\text{st}}(\varphi)$ on the intensity pattern may be evaluated as

$$\Theta_{\text{st}}(\varphi) = \Theta_0 - \frac{3}{2\left(1 + c_{14}^2/c_{44}^2\right)}\left[\frac{C_{\text{st}}^2(\varphi)}{4\,|c_{14}|\,c_{44}}\eta^2\right]^{1/3}. \tag{12}$$

It is seen that the caustic originates on the internal-refraction circle and contracts inward, as predicted in [2], at a 'rate' $\sim (ka)^{2/3}$. In case (b), when $C_\alpha(\varphi)$ changes sign with varying φ, both equations (11) and (12) are valid for each of the branches $\alpha = \text{st}$ and $\alpha = \text{ft}$ in, respectively, the opposite-lying sectors $\Delta\varphi_{\text{st}} = -\Delta\varphi_{\text{ft}}$, within which $C_\alpha(\varphi)$ is positive and not too small (allowing for $\theta_\alpha(\varphi) \sim \eta^{2/3}$). Those are the sectors, where 'the formerly intersecting'

parabolic lines link up to form smooth arches not reaching the 3-fold axis and so 'the formerly alternating' segments of caustics belonging to different branches join together to form a closed focusing pattern for each branch.

The effects discussed above can also occur in a non-centrosymmetric crystal with symmetry planes, if it has an acoustic axis $\boldsymbol{m}_{0d}$ outside of the symmetry planes so that the corresponding conical degeneracy point of the slowness sheets is lifted under spatial dispersion [8]. Unlike the case of a 3-fold axis, the local shape of disconnected slowness sheets is not spherical (the relation for the near-axial case with the principal curvatures superseding (10) for a generic orientation of $\boldsymbol{m}_{0d}$ is presented in the appendix). The behaviour of focusing caustics around $\boldsymbol{m}_{0d}$ may follow one of the two options (a) and (b) near a 3-fold axis. Apart from those, there is the possibility that in the non-dispersive limit the sheet $S_{\rm st}$ is concave and the sheet $S_{\rm ft}$ is hyperbolic everywhere around a conical point when it occurs in a non-symmetric direction $\boldsymbol{m}_{0d}$ [11]. In such a case it is the fast quasitransverse branch which under linear dispersion acquires the closed parabolic line $\theta_{\rm ft}(\varphi) \sim \eta^{2/3}$ and the corresponding phonon-focusing caustics emerge at the internal-refraction ellipse.

4. 4-fold axis

In the absence of dispersion, the slowness sheets $S_{\rm st}$, $S_{\rm ft}$ touch each other along a 4-fold axis of the elastic-tensor symmetry (this also includes a 2-fold axis in the 23 and $m3$ cubic groups). Although the contact is smooth, the principal curvatures of the degenerate sheets depend on the azimuth angle in the infinitesimal neighbourhood of the 4-fold axis, that is, the curvature at the point of degeneracy is undefined. The degeneracy point may be (a) encompassed by a region where the Gaussian curvature is of one sign; or else it may be (b) at an intersection of four parabolic lines separating adjoining domains of different Gaussian-curvature sign, which gives rise to a cross-like structure of focusing caustics. The classification of possibilities and their criteria have been established in [5, 7].

Consider the effect of linear dispersion when it is to lift the degeneracy of slowness sheets along a 4-fold axis. This specifies the symmetry groups 4, 422, 23, 432, which admit $d_{13233} \neq 0$. The perturbation-theory expansion for the phase velocities near the 4-fold axis yields [8]

$$\rho v_\alpha^2 = c_{44} + \tfrac{1}{2}\nu_3\theta^2 \mp \sqrt{\tfrac{1}{4}\left(\nu_1^2\cos^2 2\varphi + \nu_2^2 \sin^2 2\varphi\right)\theta^4 + c_{44}^2\eta^2} \qquad \alpha = \text{st, ft} \tag{13}$$

where η is defined by (9), and

$$\nu_1 = \Delta_{16} - \frac{d_{13}^2}{\Delta_{34}} \qquad \nu_2 = d_{12} - \frac{d_{13}^2}{\Delta_{34}} \qquad \nu_3 = \Delta_{14} - \Delta_{46} - \frac{d_{13}^2}{\Delta_{34}} \tag{14}$$

($\nu_1 = \nu_3 = \Delta - d^2/\Delta$, $\nu_2 = d - d^2/\Delta$ in the case of cubic media; note that the parameters ν_1, ν_3 also appear in the expansion (8) near the 3-fold axis). For $\theta \ll \eta^{1/2}$, the principal curvatures of the sheets $S_{\rm st}$, $S_{\rm ft}$ neglecting the terms $\sim \eta$ are all equal, and are given by

$$K_{1,2}^{(\rm st)} = K_{1,2}^{(\rm ft)} = \frac{1}{2\sqrt{\rho c_{44}}}\left(c_{11} + c_{66} - \frac{d_{13}^2}{\Delta_{34}}\right). \tag{15}$$

Thus, the sheets $S_{\rm st}$, $S_{\rm ft}$ become spherical and either both convex or both concave in the immediate neighbourhood of the axis. Note that any of the different possible curvature patterns, characterizing the local shape of the degenerate sheets, undergoes an abrupt change to (15) no matter how small the degeneracy-lifting perturbation η is, but then outside the critical region $\theta \sim \eta^{1/2}$ the sheets settle back to the shape well approximated by the non-dispersive limit.

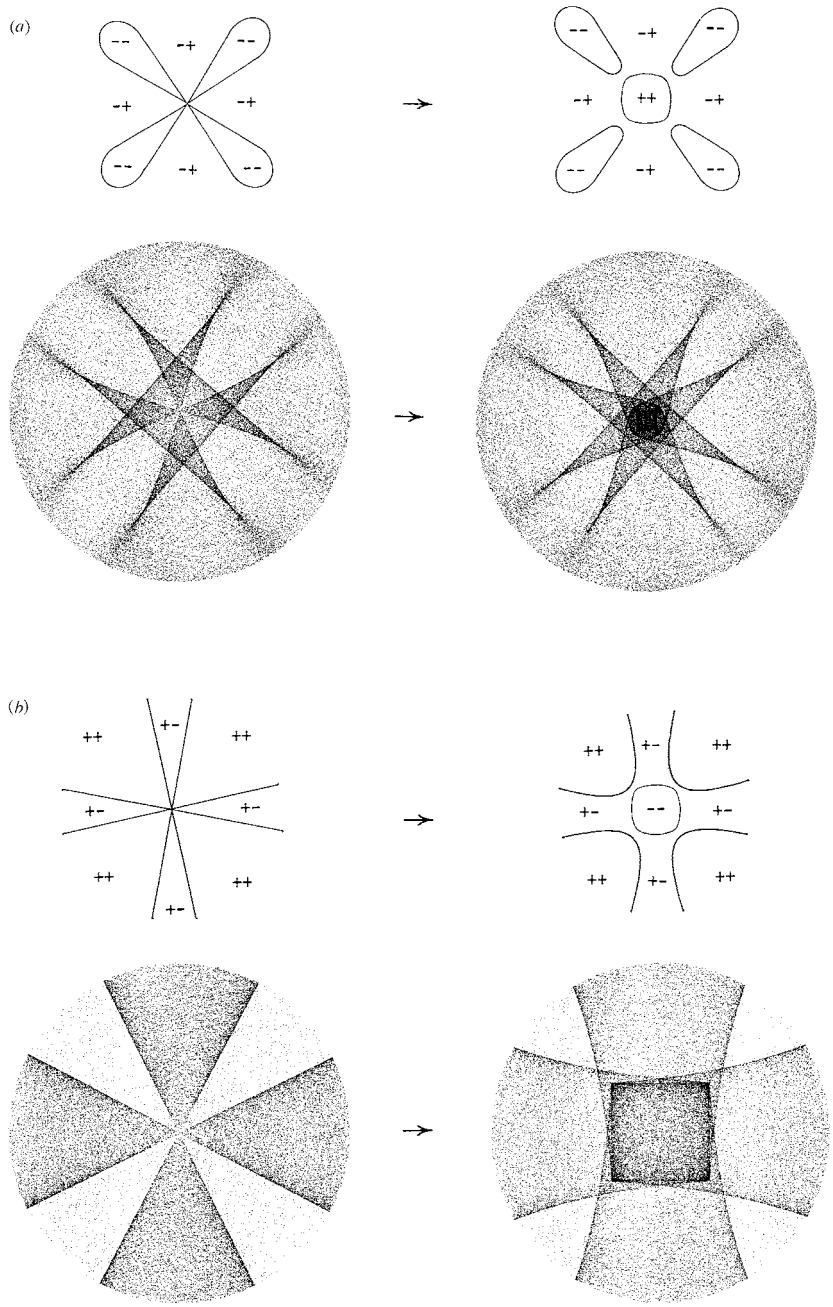

Figure 1. Possible effect of linear dispersion on the cross-like focusing caustic centred on a 4-fold axis. (*a*) Schematic variation of the near-axial curvatures of the slowness sheet S_{st} transforming under dispersion (the signs of principal curvature and the parabolic lines are indicated), and the corresponding transformation of the phonon-intensity pattern for the α = st branch at $c_{11} : c_{12} : c_{44} = 5 : 3.7 : 1$ and $\eta = 0.0043$ (the aperture angle is 4°, the darkness of the grey scale denotes intensity); (*b*) the same for the α = ft branch at $c_{11} : c_{12} : c_{44} = 2 : 1.5 : 1$.

On this basis, the salient changes of the phonon-focusing caustics near the 4-fold axis under linear dispersion can be straightforwardly predicted from knowledge of the elastic coefficients of a given crystal. In case (a), if the sign of near-axial curvatures given by (15) differs from the sign of one or both principal curvatures which conform to the non-dispersive limit, then, respectively, one or two closed parabolic lines arise and hence one or two new focusing caustics emerge. In case (b), the parabolic lines, which no longer can intersect along the 4-fold axis after degeneracy is lifted, link up at $\theta \sim \eta^{1/2}$ in either diagonal or face symmetry planes, causing focusing caustics to terminate at cuspidal points without reaching the axis. Herewith, if the near-axial shape does not match both surrounding curvature patterns, then a closed parabolic line also appears and so a new focusing caustic develops.

The options can be sorted out particularly transparently for the cubic 23 and 432 crystals by addressing the chart of the slowness-surface configurations in the non-dispersive limit plotted as lines on the plane of elastic-constant ratios $a = c_{11}/c_{44}$, $b = c_{12}/c_{44}$ [5]. In these terms, the threshold criterion for either the convex or concave dispersion-induced shape of the slowness sheets at the 4-fold axes, which by (15) is

$$a^2 - 1 - (b+1)^2 = 0 \tag{16}$$

defines another line on the above-mentioned chart (it lies between lines C and D referred to the $\alpha =$ st branch, and crosses at $b = 0$ the line H referred to the $\alpha =$ ft branch). Consider the branch $\alpha =$ st. When case (b) applies, one may observe that disconnected segments of the cross-like caustic end up in the diagonal or face symmetry planes, respectively, if $a^2 - 1 - (b+1)^2$ is positive or negative (see the example in [2]). If $a(a-1) < (b+1)^2 < a^2 - 1$ (the area between the line B and the line (16) in the chart [5]), then the new focusing caustic emerges, possibly accompanied by unfolding of the cross-like caustic. The latter event (it occurs between the lines C and (16)) is demonstrated in figure 1(a), which also confirms that the critical effect of linear dispersion on focusing caustics is confined to the close neighbourhood of the axis. For the $\alpha =$ ft branch, the following critical events are possible. In case (b), if $0 < a^2 - 1 < (b+1)^2$ (the area to the right of the line (16)), then segments of the cross-like caustic join up in the diagonal plane and this is accompanied by the emergence of a four-cusped caustic (figure 1(b)). If $\frac{1}{2}a\,(a+b) < (b+1)^2 < a^2 - 1$ (this is between the lines H and (16)), then those segments end up in the face plane and no closed caustic arises. In case (a), if $a^2 - 1 < (b+1)^2 < \frac{1}{2}a\,(a+b)$ (the region between the lines (16) and H, which exists at $b < 0$), then two new closed focusing caustics appear, as shown in figure 2. One of them is smooth and rounded, while the other one has an eight-cusped form and may be interpreted by analogy with [9] as the unfolded external conical refraction caustic.

In conclusion to this section, it is pertinent to consider one particular case related to the effect of spatial dispersion in centrosymmetric crystals. Here, the leading-order correction to the elasticity tensor c_{ijkl} is $h_{ijklpq}k_pk_q$ (quadratic dispersion). Being real and symmetric, such a perturbation cannot eliminate a polarization-vector singularity associated with phase-velocity degeneracy [12, 13], and so it cannot lift the degeneracy. It also cannot split but only shifts the conical degeneracy occurring in a non-symmetric direction. The degeneracies along symmetry axes remain intact except for the case of the $m3$ cubic group, in which the quadratic dispersion splits the tangential degeneracy along the 2-fold axes (the 4-fold axes for acoustic properties in the absence of dispersion) into two conical ones. The perturbation-theory expansion for the phase velocities gives

$$\rho v_\alpha^2 = c_{44} + \tfrac{1}{2}\nu_1\theta^2 + \zeta_+ \mp \sqrt{\left(\tfrac{1}{2}\nu_1\theta^2\cos 2\varphi + \zeta_-\right)^2 + \tfrac{1}{4}\nu_2^2\theta^2\sin^2 2\varphi} \qquad \alpha = \text{st, ft} \tag{17}$$

where $\zeta_\pm = (h_{311333} \pm h_{32233})\,k^2/c_{44} \sim (ka)^2$ is the parameter of quadratic dispersion. It is seen that the split directions of degeneracy subtend an angle $\theta \sim \zeta_-^{1/2} \sim ka$ and lie in one or

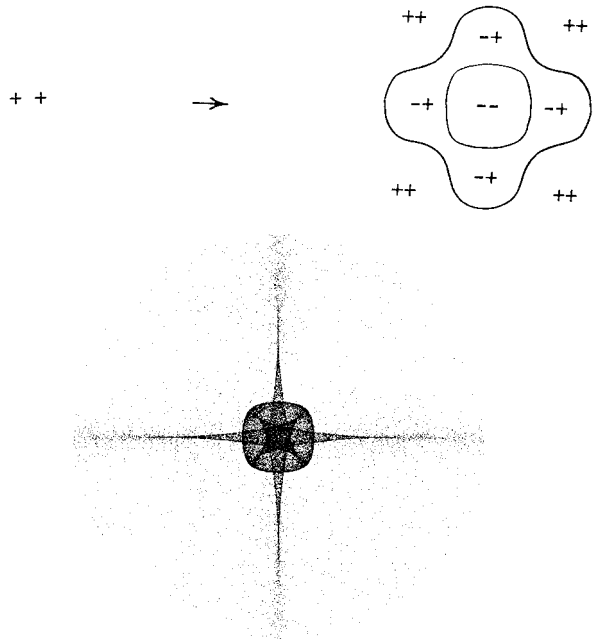

Figure 2. An example of two focusing caustics emerging around a 4-fold axis under the effect of linear dispersion: transformation of the near-axial curvatures of the slowness sheet $S_{\rm ft}$, and the corresponding phonon-intensity pattern for $c_{11} : c_{12} : c_{44} = 1.1 : -0.5 : 1$ and $\eta = 0.017$ (the aperture angle is 3°).

the other symmetry plane containing the 2-fold axis, the choice being decided by the sign of $\nu_1\zeta_-$. The slowness sheets $S_{\rm st}$, $S_{\rm ft}$, disjointed along the 2-fold axis under quadratic dispersion, acquire in its close proximity $\theta \ll \zeta_-^{1/2}$ the following principal curvatures:

$$K_1^{(\rm st)} = K_2^{(\rm ft)} = \sqrt{\frac{c_{44}}{\rho}} \qquad K_2^{(\rm st)} = K_1^{(\rm ft)} = \frac{1}{\sqrt{\rho c_{44}}}\left(c_{11} - \frac{d^2}{\Delta}\right) \tag{18}$$

where terms $\sim (ka)^2$ are neglected. Thus, the sheets $S_{\rm st}$, $S_{\rm ft}$ along the 2-fold axes in the $m3$ group are either both convex or both hyperbolic when dispersion is at work. The threshold criterion, given in the a, b notation by

$$a\,(a-1) - (b+1)^2 = 0 \tag{19}$$

coincides with the equation of the line B in the chart [5]. This facilitates a straightforward prediction of the critical effects of quadratic dispersion on the phonon-focusing pattern of a cubic $m3$ crystal. In case (a), the new focusing caustic appears for the $\alpha =$ st branch if $0 < (a+b)\,(a-1) < (a-b-2)\,(b+1)^2$ (which is to the right of the line D, where the new hyperbolic region borders at $\theta \sim ka$ with the concavity on $S_{\rm st}$); and the new caustic appears for the $\alpha =$ ft branch if $a\,(a-1) < (b+1)^2 < \frac{1}{2}a\,(a+b)$ (this is between the lines B and H, so the hyperbolic region convexity is surrounded by the convexity on $S_{\rm ft}$). Regarding case (b), we note that the cross-like caustic may unfold by means of two pairs of parabolic lines merging together in a strip which pushes apart two other pairs (figure 4). This reveals the 2-fold (rather than the 4-fold) symmetry of the axis unveiled in the presence of quadratic dispersion.

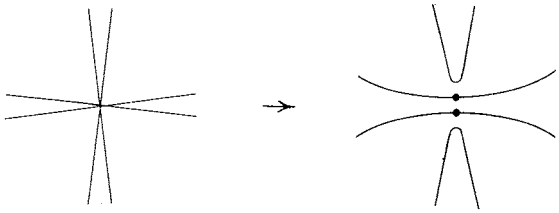

Figure 3. A pattern of transformation of the parabolic-lines intersection under the effect of quadratic dispersion in an $m3$ cubic crystal (conical points are marked).

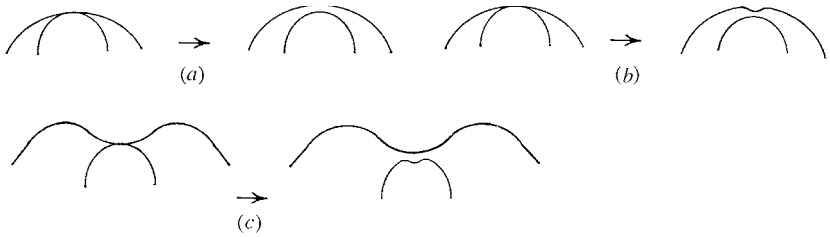

Figure 4. Near-axial shape of the slowness sheets coming apart along a 6-fold axis under the effect of linear dispersion.

5. 6-fold axis

Due to the transverse isotropy of the elastic constants ($\nu_1 = \nu_2$ in (13)), the point of tangential degeneracy along a 6-fold axis is a regular point of the slowness sheets, with well defined principal curvatures [7, 14]

$$\begin{aligned} K_{1,2}^{(\mathrm{st})} &= \frac{c_{66}}{\sqrt{\rho c_{44}}} \qquad K_{1,2}^{(\mathrm{ft})} = \frac{1}{\sqrt{\rho c_{44}}}\left(c_{11} - \frac{d_{13}^2}{\Delta_{34}}\right) \qquad \text{if} \quad \Delta_{16} > \frac{d_{13}^2}{\Delta_{34}} \\ K_{1,2}^{(\mathrm{st})} &= \frac{1}{\sqrt{\rho c_{44}}}\left(c_{11} - \frac{d_{13}^2}{\Delta_{34}}\right) \qquad K_{1,2}^{(\mathrm{ft})} = \frac{c_{66}}{\sqrt{\rho c_{44}}} \qquad \text{if} \quad \Delta_{16} < \frac{d_{13}^2}{\Delta_{34}}. \end{aligned} \tag{20}$$

However, when linear dispersion lifts the degeneracy, which is the case for the groups 6 and 622, the near-axial shape abruptly changes in the same fashion as in the above-considered case of a 4-fold axis. In effect, the curvature singularity at the degenerate point along a 6-fold axis is suppressed in the absence of dispersion, but it reveals itself when degeneracy is removed (albeit the transverse isotropy persists). For $\theta \lesssim \eta^{1/2}$, the in-plane principal curvature $K_1^{(\alpha)}(\theta)$ (the one referred to the section by a zonal plane through the 6-fold axis) is approximated by

$$K_1^{(\alpha)}(\theta) = \frac{1}{2\sqrt{\rho c_{44}}}\left[\nu_1 + 2c_{66} \mp \frac{\nu_1^2\theta^2\left(\nu_1^2\theta^4 + 12c_{44}^2\eta^2\right)}{\left(\nu_1^2\theta^4 + 4c_{44}^2\eta^2\right)^{3/2}}\right] \qquad \alpha = \mathrm{st}, \mathrm{ft} \tag{21}$$

and the transverse principal curvature $K_2^{(\alpha)}(\theta)$ by

$$K_2^{(\alpha)} = \frac{1}{2\sqrt{\rho c_{44}}}\left[\nu_1 + 2c_{66} \mp \frac{\nu_1^2\theta^2}{\left(\nu_1^2\theta^4 + 4c_{44}^2\eta^2\right)^{1/2}}\right] \qquad \alpha = \mathrm{st}, \mathrm{ft}. \tag{22}$$

This leads to (15) at $\theta = 0$ and to (20) at $\theta \gg \eta^{1/2}$ ($\theta \ll 1$), whose combination in a given crystal determines the evolution of the local shape of its slowness surface due to linear dispersion. If

$$c_{11} - d_{13}^2/\Delta_{34} > 0 \tag{23}$$

then both sheets $S_{\rm st}$, $S_{\rm ft}$ stay convex for $\theta \ll 1$ (figure 4(a)), and no critical effects occur in the phonon-intensity pattern. If

$$c_{11} - \frac{d_{13}^2}{\Delta_{34}} < 0 \qquad c_{11} + c_{66} - \frac{d_{13}^2}{\Delta_{34}} > 0 \tag{24}$$

then the inner sheet $S_{\rm ft}$ still stays convex throughout the range $\theta \ll 1$, whereas the outer sheet $S_{\rm st}$ acquires two circular parabolic lines of an angular size $\theta_{\rm st1}, \theta_{\rm st2} \sim \eta^{1/2}$ (figure 4(b)). The first one, at which $K_1^{(\rm st)}(\theta) = 0$, separates the axial concavity from the domain of hyperbolic points, and then the second one, at which $K_2^{(\rm ft)}(\theta) = 0$, separates the intermediate hyperbolic belt from the exterior convexity. The latter parabolic line, evaluated by the equation

$$\theta_{\rm st2}^4 = \eta^2 \frac{c_{44}^2 \Delta_{34} \left[(c_{11} + c_{66})\, \Delta_{34} - d_{13}^2 \right]^2}{c_{66} \left(\Delta_{16} \Delta_{34} - d_{13}^2 \right)^2 \left(d_{13}^2 - c_{11} \Delta_{34} \right)} \tag{25}$$

defines the cone of wave normals which all have the same group-velocity vector parallel to the 6-fold axis. This leads to the phenomenon known as external conical refraction, which in case (24) is induced by linear dispersion. Lastly, if

$$c_{11} + c_{66} - \frac{d_{13}^2}{\Delta_{34}} < 0 \tag{26}$$

then the sheet $S_{\rm st}$ stays concave within the whole range $\theta \ll 1$ and exhibits external conical refraction which is only slightly disturbed in comparison with the non-dispersive limit (see [14, 15]). At the same time, it is now the inner sheet $S_{\rm ft}$, which under the effect of linear dispersion becomes concave around the 6-fold axis and so gains two parabolic lines of an angular size $\theta_{\rm ft1}, \theta_{\rm ft2} \sim \eta^{1/2}$ (figure 4(c)). The latter line, for wave normal directions $\theta_{\rm ft2}$ defined by the same right-hand side (25), gives rise to the dispersion-induced external conical refraction for the fast quasitransverse waves, which appears against the background of the non-dispersive external conical refraction of the slow quasitransverse waves.

6. Experimental realizability

Linear spatial dispersion of phonons and ultrasound have been observed in crystals with a number of techniques, including inelastic neutron scattering, Brillouin scattering, acoustic activity and Bragg reflection of light. The aforementioned techniques probe the acoustic dispersion relation $\omega(k)$ and, in particular, the splitting that occurs between the ST and FT constant-frequency sheets at acoustic axes and its linear increase with frequency. To directly access the wave surface, its folds and associated energy focusing caustics, and the evolution of these with frequency, requires transport measurements either with ultrasound or thermal phonons.

The ultrasound experiments that in the past have been brought to bear on the study of focusing have operated from 5 to 382 MHz. At the lower end of this frequency range, internal diffraction effects obliterate all but the dominant focusing structures, and even at the higher frequencies, diffraction tends to obscure finer caustic structures of the type discussed in this paper. To overcome this obstacle, significantly higher frequencies and/or larger samples would be required.

The most promising avenue at present for observing the structures discussed here is with thermal phonons in the frequency range around 100–500 GHz. In phonon-imaging experiments, which display the directional dependence of the phonon flux emanating from a small heated spot which is raster scanned across the surface of a crystal, focusing caustics are

revealed in striking detail. These experiments are conducted at liquid helium temperatures, under which conditions thermal phonon mean free paths are comparable to or larger than the sample's dimensions, so that the phonon transport is ballistic rather than diffusive. For detection, small superconducting bolometers are used, which measure the total incident energy flux of phonons, while frequency selectivity is achievable with the use of superconducting tunnel junction detectors.

There is an extensive literature (reviewed in [1]) on the phonon images of crystals both for lower-frequency non-dispersive phonons and for large-wavevector strongly dispersive phonons. The subject matter of the present paper concerns the intermediate-frequency range where dispersive effects first make their appearance, and under the conditions described earlier, are linear in frequency. This regime for quartz has been explored experimentally by Koos *et al* [17] and theoretically by Every [2]. There was only limited frequency resolution in the experiments, and the observed phonon focusing patterns were the superposition of focusing patterns over a range of frequencies. Nevertheless, clear structures survived, albeit not as sharp as non-dispersive caustics.

The angular resolution which is achievable in phonon imaging (e.g. Shields *et al* [18] report measurements on a caustic in silicon to 0.09°) is sufficient to reveal the main structures contained in the calculated images in figures 1 and 2, which extend over 3°–4° of arc.

Acknowledgments

Financial support for this project has been provided by the South African National Research Foundation, and the Russian Foundation for Fundamental Research (grant no 97-02-16338).

Appendix

Consider an arbitrary non-centrosymmetric crystal (barring cubic and hexagonal ones), and assume an acoustic axis $\boldsymbol{m}_{0d}$ which is neither parallel to a symmetry axis nor lies in a symmetry plane. The perturbation-theory expansion for the phase velocities at $\boldsymbol{m} \approx \boldsymbol{m}_{0d} + \theta \boldsymbol{e}_\varphi$ ($\boldsymbol{m}_{0d} \cdot \boldsymbol{e}_\varphi = 0, \theta \ll 1$) gives [8]

$$\rho v_\alpha^2 = \rho v_{0d}^2 + 2\rho v_{0d} \boldsymbol{w} \cdot \boldsymbol{e}_\varphi \theta \mp \sqrt{\left[(\boldsymbol{p} \cdot \boldsymbol{e}_\varphi)^2 + (\boldsymbol{q} \cdot \boldsymbol{e}_\varphi)^2\right]\theta^2 + \left(\rho v_{0d}^2 \eta\right)^2} \qquad \alpha = \text{st, ft.} \quad \text{(A1)}$$

Here

$$\begin{aligned} \boldsymbol{w} &= \frac{1}{2v_{0d}} \left(\boldsymbol{A}_{01} \boldsymbol{c} \boldsymbol{A}_{01} + \boldsymbol{A}_{02} \boldsymbol{c} \boldsymbol{A}_{02}\right) \boldsymbol{m}_{0d} \\ \boldsymbol{p} &= \left(\boldsymbol{A}_{01} \boldsymbol{c} \boldsymbol{A}_{01} - \boldsymbol{A}_{02} \boldsymbol{c} \boldsymbol{A}_{02}\right) \boldsymbol{m}_{0d} \qquad \boldsymbol{q} = \left(\boldsymbol{A}_{01} \boldsymbol{c} \boldsymbol{A}_{02} + \boldsymbol{A}_{02} \boldsymbol{c} \boldsymbol{A}_{01}\right) \boldsymbol{m}_{0d} \end{aligned} \quad \text{(A2)}$$

are the vectors describing the elliptical cone of internal refraction in the non-dispersive limit [16]: $\boldsymbol{w}$ connects its apex with the centre of the base, and $\boldsymbol{p}, \boldsymbol{q}$ determine the lengths of base semiaxes ($\boldsymbol{A}_{01}, \boldsymbol{A}_{02}$ denote arbitrary unit vectors which make a rectangular frame with the polarization vector $\boldsymbol{A}_{03}$ of the non-degenerate wave propagating along $\boldsymbol{m}_{0d}$, and $\boldsymbol{A}_{0\alpha} \boldsymbol{c} \boldsymbol{A}_{0\beta} \boldsymbol{m}_{0d} \equiv c_{ijkl} \left(A_{0\alpha}\right)_i \left(A_{0\beta}\right)_k \left(m_{0d}\right)_l$). The spatial-dispersion parameter η, lifting the degeneracy, is defined with respect to arbitrary anisotropy as

$$\eta = \frac{\omega}{\rho v_{0d}^3} \left| d_{ijklp} \left(m_{0d}\right)_j \left(m_{0d}\right)_l \left(m_{0d}\right)_p \left(A_{01}\right)_i \left(A_{02}\right)_k \right|. \quad \text{(A3)}$$

In the very close neighbourhood of the acoustic axis $\boldsymbol{m}_{0d}$, such that $\theta \ll \eta \sim ka$, the group-velocity vectors of the disconnected branches $\alpha =$ st, ft are approximately (in neglect of terms

$\sim\eta$) equal to $\boldsymbol{w}$, and the principal curvatures of the separated slowness sheets to leading order are

$$K_{1,2}^{(\mathrm{st})} = -K_{1,2}^{(\mathrm{ft})} = -\frac{1}{4\eta\,|\boldsymbol{w}|^3\,\rho^2 v_{0d}^2}\left\{(\boldsymbol{w}\times\boldsymbol{p})^2 + (\boldsymbol{w}\times\boldsymbol{q})^2 \right.$$
$$\left. \pm\sqrt{\left[(\boldsymbol{w}\times\boldsymbol{p})^2 + (\boldsymbol{w}\times\boldsymbol{q})^2\right]^2 - 4\boldsymbol{w}^2 v_{0d}^2\,(\boldsymbol{p}\times\boldsymbol{q})^2}\right\} \tag{A4}$$

where $\times$ denotes a vector product; the alternative signs correspond to the different principal curvatures of each sheet. It is readily confirmed that $K_{1,2}^{(\mathrm{st})} < 0$, $K_{1,2}^{(\mathrm{ft})} > 0$. The Gaussian curvature given by (A4) is

$$K_G^{(\mathrm{st})} = K_G^{(\mathrm{ft})} = \frac{(\boldsymbol{p}\times\boldsymbol{q})^2}{4\eta^2\rho^4\boldsymbol{w}^4 v_{0d}^2}. \tag{A5}$$

Equation (A4) becomes (10) for $\boldsymbol{w}\times\boldsymbol{m}_{0d} = 0$, hence $\boldsymbol{w}^2 = v_{0d}^2$ and $\boldsymbol{w}\cdot\boldsymbol{p} = \boldsymbol{w}\cdot\boldsymbol{q} = 0$.

Note that $\boldsymbol{p}\times\boldsymbol{q} = 0$ along the line of intersection of the slowness sheets (line of wedge degeneracy), which is common for hexagonal crystals [16]. Given that linear dispersion lifts this degeneracy ($\eta \neq 0$, the groups 6, 622), equation (A4) reveals a large value of the in-plane curvature $K_1^{(\mathrm{ft})} = -K_1^{(\mathrm{st})} \sim 1/\eta$ at the rounded points of disconnected sheets. Equation (A5) is not valid in this case, since the transverse curvature is to be evaluated from the next-order term, for which critical dependence on the dispersion parameter η cancels out.

References

[1] Wolfe J P 1998 *Imaging Phonons* (Cambridge: Cambridge University Press)
[2] Every A G 1987 *Phys. Rev.* B **36** 1448
[3] Portigal D L and Burstein E 1968 *Phys. Rev.* **170** 673
[4] DiVincenzo D P 1986 *Phys. Rev.* B **34** 5450
[5] Every A G 1981 *Phys. Rev.* B **24** 2852
[6] Maris H J 1986 *Nonequilibrium Phonons in Nonmetallic Crystals* ed W Eisenmenger and A A Kaplyanskii (Amsterdam: North-Holland) p 51
[7] Shuvalov A L and Every A G 1996 *Phys. Rev.* B **53** 14 906
[8] Shuvalov A L 1998 *J. Acoust. Soc. Am.* **104** 2008
[9] Every A G 1986 *Phys. Rev.* B **34** 2852
[10] Khatkevich A G and Kurilkina S N 1988 *Sov. Phys. Solid State* **30** 786
[11] Shuvalov A L and Every A G 1997 *J. Acoust. Soc. Am.* **101** 2381
[12] Alshits V I, Sarychev A V and Shuvalov A L 1985 *Sov. Phys.–JETP* **62** 531
[13] Shuvalov A L 1998 *Proc. R. Soc.* A **454** 2911
[14] Musgrave M J K 1970 *Crystal Acoustics* (San Francisco, CA: Holden-Day)
[15] Kim K Y, Sachse W and Every A G 1993 *Phys. Rev. Lett.* **70** 3434
Kim K Y, Every A G and Sachse W 1994 *Int. J. Mod. Phys.* B **8** 2327
[16] Fedorov F I 1968 *Theory of Elastic Waves in Crystals* (New York: Plenum)
[17] Koos G L and Wolfe J P 1984 *Phys. Rev.* B **30** 3470
[18] Shields J A and Wolfe J P 1989 *Z. Phys.* B **75** 11